A surface-shunting method for the prevention of a fault-mode-induced quench in high-field no-insulation REBCO magnets

Fangliang Dong, Dongkeun Park*, Junseong Kim, Juan Bascuñán, and Yukikazu Iwasa
Francis Bitter Magnet Laboratory/Plasma Science and Fusion Center, Massachusetts Institute of Technology, Cambridge, MA 02139, USA (*e-mail: dk_park@mit.edu).

Abstract

In this paper, we apply a surface-shunting method to prevent quenches in no-insulation (NI) REBCO magnets triggered by external failures of magnet current leads or power suppliers (i.e., fault mode). In a high-field magnet system, an NI coil may still be at risk during the mentioned quench events even if the whole magnet is well-designed, non-defective, and properly operated. The mechanism of this fault-mode quench initiation and propagation still remains unclear, complicating the development of reliable quench protection. Here, we present this mechanism to demonstrate a corresponding practical quench-preventive approach named surface shunting, which utilizes a low-temperature solder attached to the top and bottom of pancake coils. We validate the effectiveness of this approach by comparing the electromagnetic, thermal, and mechanical behaviors in the fault mode with and without the shunt. We conclude that the surface shunt suppresses the fault-mode quench initiation and propagation by redirecting the original turn-to-turn current and induced overcurrent out of the NI winding. We anticipate this work can provide a solution to improve the operational safety of high-field HTS NI magnets against quench and potential damage during fault modes.

Keywords: HTS magnet; No insulation; Electrical shunt; Quench protection.

1. Introduction

High-temperature superconducting (HTS) magnets have been designed and constructed as key components in various applications such as compact nuclear fusion reactors, high-power-density electrical motors/generators, high-resolution NMR/MRI, and state-of-the-art high-energy physics experiments[1-7], based on their capability of carrying bulk supercurrent and generating high magnetic fields. To date, several high-field HTS magnets have been successfully built, and the record for the achieved field has been increasing steadily. From HTS-Bitter magnets of 26.8 T in 2009[8] to 40.2 T in 2016 and 45.5 T in 2017, reported in 2019[9], and all-superconducting magnets of 32.25 T in 2020[10]. However, an HTS magnet could unexpectedly quench, caused by both internal and external disturbances such as conductor defects, AC losses during the electromagnetic transients, cryogenic cooling, power supplying failures, and nuclear heat load in fusion magnets, etc[11, 12]. This quenching issue, characterized by a drastic and uncontrollable collapse of stored energy, can result in irreversible damage to the magnets. Quench

protection, with safely releasing large amounts of stored energy, remains a tough and critical issue due to the difficulty in detecting the slowly propagating normal zone, e.g., ~15 mm/s[13, 14], at the early stages of a quench in HTS magnets.

The no-insulation (NI) winding technique, which involves removing turn-to-turn insulation, has been demonstrated to be self-protective against overcurrent and overheating[15-18]. In the case of a hot spot occurrence, this dissipative normal region can be bypassed by current transferring to adjacent turns[19, 20], significantly reducing the quench risk by preventing overheating and consequential permanent burn-out. The NI technique is regarded as a promising self-protective approach for various applications including electrical power devices[21], efficient transportation[22-24], compact nuclear fusion reactors[25, 26], and NMR spectrometers[27, 28].

There is still evidence of mechanical damage to some NI magnets that could cause or result from a quench[9, 29-31]. The NI magnet quenches reported so far have mostly occurred during energization[29, 30, 32, 33] and appear to be caused by internal defects in conductors or coil design/construction. These defects can theoretically be avoided by using non-defective conductors, designing with a more conservative margin, and constructing magnets through a careful and reliable process, among other measures[18, 27, 34-37].

However, we have experienced that even with well-designed, non-defective, and well-operated NI magnets, still there is a kind of quench that can occur under certain specific external operating fault mode. The specific fault mode includes failures external to the magnet itself, such as failures of the current leads or the power supply, resulting in an open current loop, suddenly dropping the current flow through the magnets. We differentiate these fault-mode quenches from the above internal-defect-induced quenches caused by conductor and/or winding defects. Particularly, these quenches occurred in NI HTS magnets, especially the compact high-field ones operating with high current density at low temperatures to maximize the magnet performance and cost-effectiveness, can severely damage the magnets as shown in our previously constructed 18.8-T 3-coil nested NMR magnet[30, 33, 38] and other fusion magnets[1, 39]. To date, besides our preliminary work done in 2022[40, 41], these specific externally induced quenches in NI coils, especially at the magnet level with more complicated electromagnet coupling, have not yet been extensively studied, nor have the corresponding preventive approaches. It is necessary to enhance the robustness of magnets against the fault-mode quenches for the safe operation of large-scale and/or high-field NI magnet systems.

In this work, we examine the externally induced fault-mode quench, including its initiation and propagation, and based on the quench mechanism, demonstrate a countermeasure of surface-shunting to improve the turn-to-turn coupling of the high-field NI REBCO magnet with the intention of making the coils robust to this type of quench. Here, we use one of our high-field HTS insert magnets currently under development as a case study, but the findings are not limited to this specific magnet. In brief, in a magnet composed of a stack of coils, the surface shunt relies on eutectic metallic compounds melting and attaching to the top and bottom of each coil to form micron-scale thin layers. This provides an effective and direct electrical bypass, in addition to the original turn-to-turn bypass, enabling better

suppression of quench initiation and interruption of propagation. Although we have preliminarily mentioned the surface-shunting approach during a construction of a lab-level magnet [42], there are no in-depth analyses on how the surface shunt works in the fault-mode quench prevention that we intend to do in this work.

This work is organized as follows: First, we introduce the study objects – a high-field REBCO magnet and the making process of the surface shunt; Next, we acquire necessary real parameters for a simulation model from experimental tests on one coil of the magnet; Finally, we use this simulation model to compare the multi-physics behaviors in the high-field magnet with and without the surface shunt to illustrate how the surface shunt prevents the fault-mode quench.

2. The magnet/coil with the surface shunt

The 1.3-GHz NMR LTS/HTS magnet (Fig.1) that we are developing at MIT, is a high-field system composed of a REBCO magnet (H835) supplying 19.65 T/835 MHz inserted in a NbTi background magnet (L500) that provides 11.74 T/500 MHz[28]. The two magnets (H835 + L500) are connected in series under a rated operating current of 230 A at 4.2 K. H835 has an inductance of over 20 H, and the full magnet has a total inductance of 203.3 H. The total energy stored in the magnet is ~6 MJ. H835 is composed of a stack of 40 double-pancake coils (DPs) from top DP1 to bottom DP40[27]. Each DP is co-wound with 4 mm × 65 μm NI REBCO conductor tapes manufactured by SuperPower Inc. and 4 mm × 50.8 μm stainless steel tapes, under winding tensions of 2.6 kg-f and 2 kg-f, respectively. The HTS conductor tape includes 50-μm Hastelloy C-276 substrate, 1-μm REBCO, ~4-μm buffer layers, a thin silver coating, and a final hermetic 5-μm electroplated copper stabilizer on each side. The REBCO layer is wound facing radially inwards to provide compressive bending strain to minimize the overall strain produced by the tensile Lorentz forces.

Both the upper and bottom surfaces of the DPs in H835 are surface shunted by low-temperature solder, as shown in Fig.2. In this work, we used Cerrolow 136 ($Bi_{49}Pb_{18}In_{21}Sn_{12}$), which has a melting point of 58 ºC [43, 44]. During the shunting process, it is crucial to remove the oxidized layer on each DP top and bottom surfaces with acetone, then slowly warm the DP up to ~80 ºC by a heat plate for ~20 minutes before applying the Cerrolow 136. Soldering flux is used to help the melted Cerrolow 136 to better attach to the DP surfaces. The excess melted shunt is wiped away in order to only retain a very thin layer on the DP surfaces.

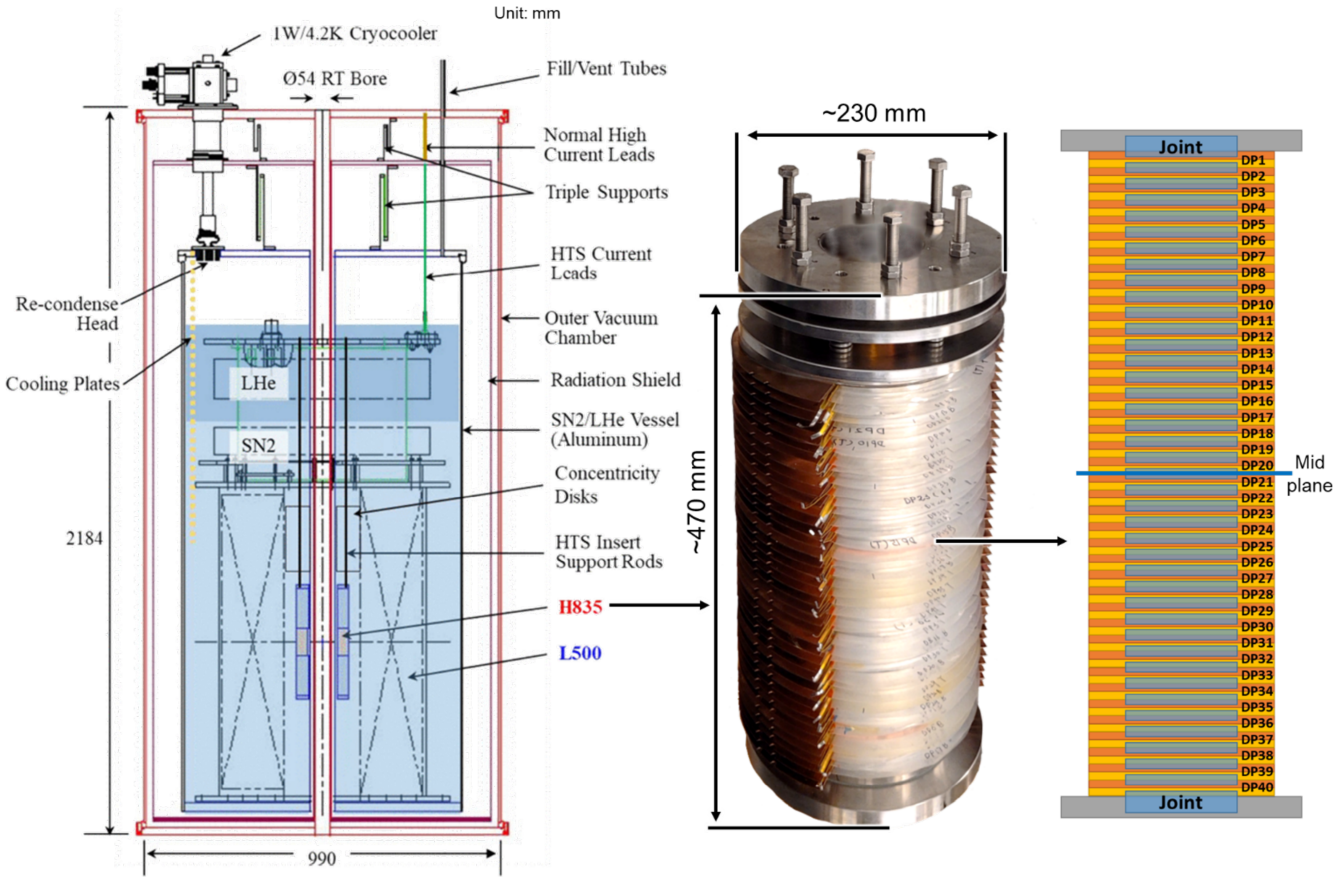

Fig.1 The HTS/LTS 1.3-GHz NMR magnet system.

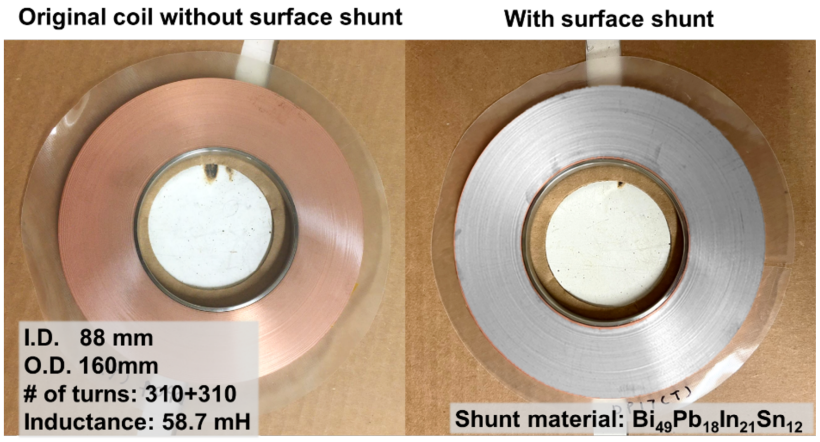

Fig.2 The surface-shunted NI double-pancake coil (DP) in the H835 REBCO magnet.

3. The experiments to acquire necessary parameters for the simulation input

In this section, we wind a DP (named DP0) completely identical to the DPs in H835, and test the DP0 under fault mode (Fig.3) to acquire essential parameters necessary for the input of a finite-element simulation model, such

as the equivalent turn-to-turn characteristic resistances with and without the shunt. DP0, the single DP representing one of the stack that makes the H835, allows us to get real parameters for more realistic results that will follow during the simulation of the entire H835 magnet.

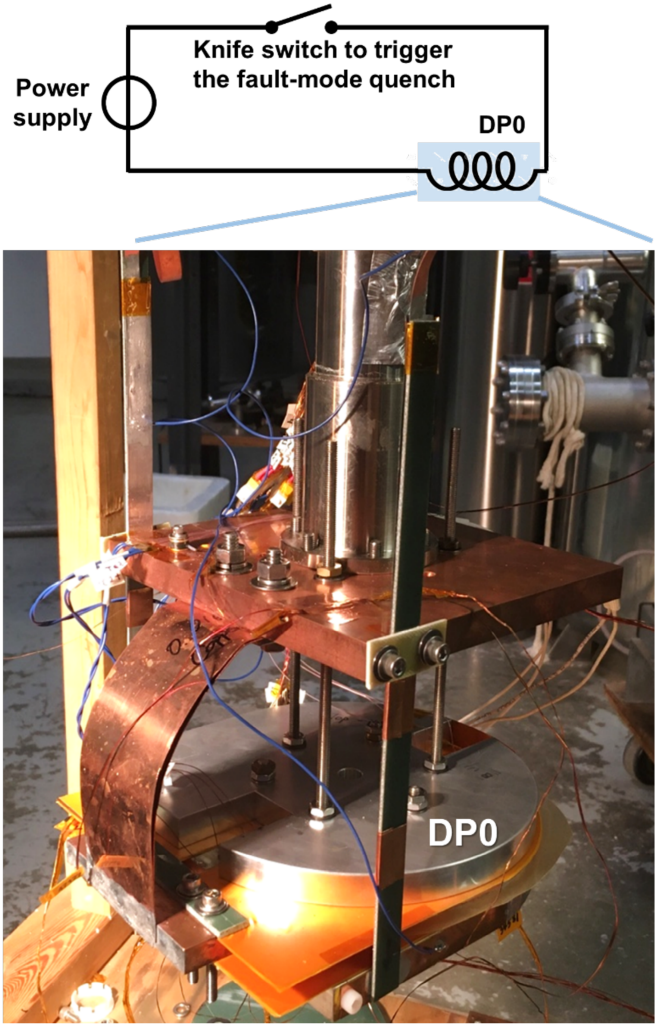

Fig.3 The setup for DP0 fault-mode test.

The finite-element simulation model for the NI HTS coils uses rotated anisotropic resistivity. This model has been explained and validated by both our group and many others[41, 45-51]. Briefly, it is built based on the frame of homogenized *H*-formulation[52] for electromagnetic features, solid heat transfer for temperature features, and solid mechanics for force/stress features. The anisotropic transition matrix **T** (Eq.1), described in Fig.4, is the key feature in the model to approximate the round coil with discrete spiral turns by a homogenized hollow co-axial pancake, while also enabling radial turn-to-turn bypassing current flow in NI coils to reproduce the unique charging/discharging behaviors. For the shunt, we build extra resistive layers covered on the coil surfaces (Fig. 5), exactly as the practical surface shunts do.

$$\begin{cases} \begin{bmatrix} r \\ \theta \\ z \end{bmatrix} = \mathbf{T} \begin{bmatrix} R \\ \Phi \\ Z \end{bmatrix} = \begin{bmatrix} \cos(\alpha) & -\sin(\alpha) & 0 \\ \sin(\alpha) & \cos(\alpha) & 0 \\ 0 & 0 & 1 \end{bmatrix} \begin{bmatrix} R \\ \Phi \\ Z \end{bmatrix} \\ \alpha = \tan^{-1}\left(\dfrac{d}{2\pi r}\right) \end{cases} \quad (1)$$

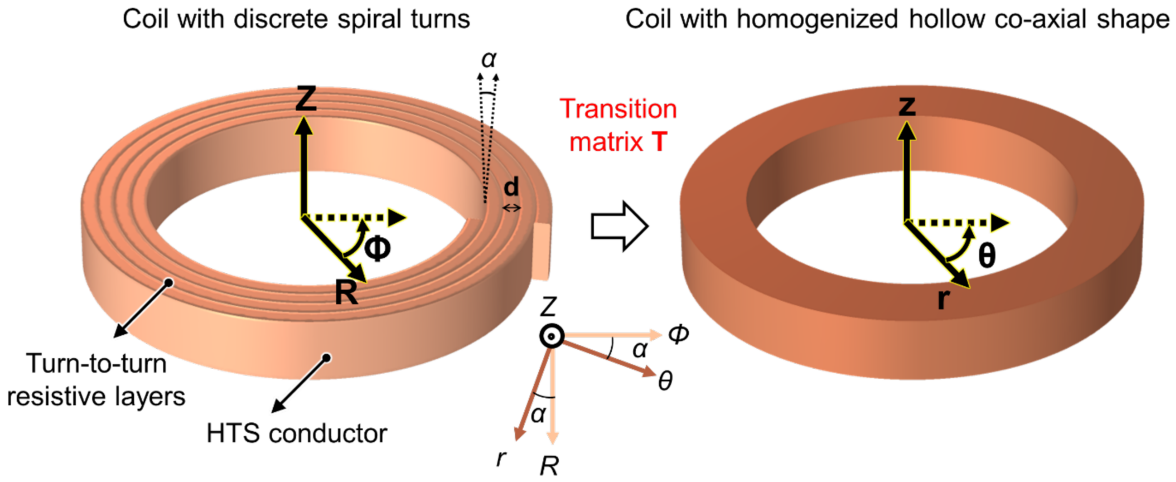

Fig.4 The anisotropic transition matrix **T** to approximate a round coil with discrete spiral turns by a homogenized hollow co-axial pancake. α is the small angle staggers between the normal-tangential unit vectors (Φ and R) and the cylindrical unit vectors (θ and r). d is the co-wind turn thickness.

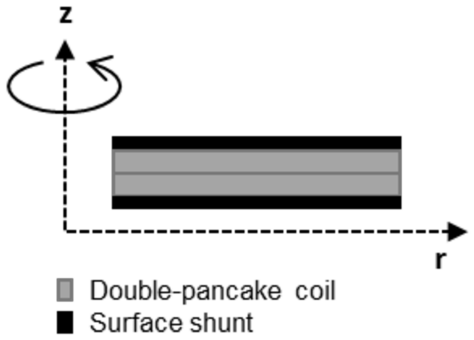

Fig.5 The schematic structure of the surface shunt in the simulation model (not to scale).

In the DP0 fault-mode test at ~4.2 K, we wait for the DP0 current and temperature to fully settle, then intentionally cut off the supplying current to the coil by using a knife switch to trigger the fault mode, causing the source current through the DP0 to step down to zero. The data acquisition rate was 1000 Hz realized by the National Instruments SCXI-1125 and PCI modules with an in-house developed Labview code. Fig.6 shows the experiment and simulation results, which match well in both unshunted (i.e., original NI) and shunted cases. Thus, we consider that the essential parameters are measured accurately for the model input to reflect the quench and the shunting processes.

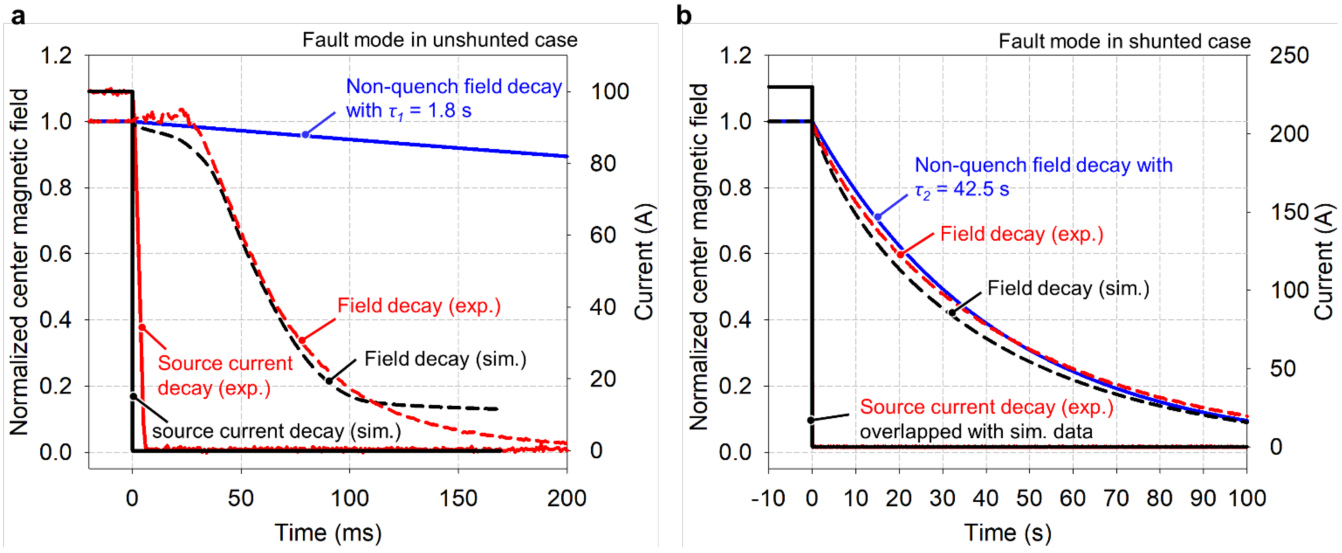

Fig.6 The test and simulation results of the fault-mode DP0 (a) without (i.e., original NI) and (b) with the surface shunts.

In the unshunted case, we charged the DP0 to 100 A ($Ic \approx 250$ A) and then cut the power supply, the DP0 immediately quenched with its measured center field decaying to 0 within ~200 ms, which is much faster than the expected time constant τ_1 = 1.8 s measured in a non-quench *R-L* decay ($\tau = L/R$, *L*: coil inductance, *R*: turn-to-turn bypass resistance[53]). In the shunted case, we charged DP0 to 230 A and then triggered the fault mode, both the simulated and the measured field decays fit well with the ideal *R-L* decay having τ_2 = 42.5 s, indicating that the shunted DP0 discharged without quench. The shunted DP0 slowly discharges the field (i.e., stored energy) and remains unquenched even at a higher initial current (230 A vs. 100 A of the unshunted case). Based on τ_1 and τ_2, we calculate that the equivalent turn-to-turn bypass resistances are R_{tt1} = 32.6 mΩ in the unshunted case and R_{tt2} = 1.38 mΩ in the shunted case. R_{tt1} also equals the turn-to-turn resistance, while R_{tt2} is a combination of R_{tt1} and shunt resistance (1.44 mΩ). The corresponding characteristic resistivity[54] is calculated to be R_{ct1} = 795 μΩ•cm^2 and R_{ct2} = 33.7 μΩ•cm^2, respectively, by Eq.2 (N_t: number of coil turns, r_i: turn radius, w_d: conductor width). R_{ct2} is ~23 times smaller than R_{ct1} because of the parallel bypass contributed by the shunt.

$$R_{ct} = \frac{R_{tt}}{\sum_{i=1}^{N_t} \frac{1}{2\pi r_i w_d}} \quad (2)$$

4. Simulation on electromagnetic and thermal behaviors with and without the shunt

In this section, we use the above model to simulate and understand the electromagnetic and thermal behaviors in the H835 magnet during the fault mode, and compare the cases with and without the surface shunt.

Fig.7a shows the distribution of the normalized transport current density to the local critical current density (*J*/*Jc*)

during the normal zone propagation in the fault-mode quench of the originally designed H835 stacked with unshunted DP coils. J/Jc >1 indicates local quench occurs as the transport current density surpasses the critical current density. The fault-mode quench starts from the end coils of the magnet. This is because the end coils have stronger magnetization and lower critical current margins as compared to the middle coils, meanwhile, the end coils have weaker electromagnetic coupling (i.e., lower mutual inductance). This results in more radial current flow warming up the winding, further decreasing the critical current density and prompting the local quench. Fig.7b shows the normal-zone propagation distance (NPD) from the end to the middle of H835 and the corresponding normal-zone propagation velocity (NPV). NPV increases as the quench propagates, and reaches the maximum of ~4m/s when entering the "energy collapse stage" which indicates the entire quench of H835. We further simulate the azimuthal current induction in each of the DP coils in H835 (from top to middle: DP1 to 20), as shown in Fig.8. When the fault mode occurs, the current in DP1-5 decays because of NI turn-to-turn dissipation, then after DP6, the induced current exceeds the original rated current of 230 A. The induced current soon reaches the corresponding critical current and quenches the coil immediately, resulting in another higher induced current in the adjacent DP coil because of magnetic flux conservation. Therefore, the normal zone spreads out by the induced overcurrent cascading as the DP coils quench one by one toward the center of the magnet. At last, the magnetic field suddenly decreases when all the DP coils quench, as shown in Fig.9. Further temperature simulation (Fig.10) shows the end coils (e.g., DP1) are warmed up earlier than the middle coils, but the middle ones have a higher final temperature, especially DP20 showing a temperature burst over 100 K at the "energy collapse stage".

The simulation shows that the fault-mode quench is triggered by heat from the turn-to-turn bypass current in the end coils of the magnet, then spreads out to the middle magnet by magnetic coupling (i.e., high induced overcurrent). As this seems to be contradictory to the self-protecting nature during NI magnet quench, we further analyze this phenomenon: Usually, the NI self-protection, based on current sharing through turn-to-turn, allows the coil to recover under transient disturbances or maintain supercurrents until the stored energy is dissipated out. However, this only works when the joule heating from bypassing currents is sufficiently removed by cooling to keep the winding temperature below the current sharing temperature (J_t/J_c<1). Here in the fault-mode quench, several end coils have gone normal, but the current keeps flowing through them, further increasing the temperature, and forcing the quench to grow.

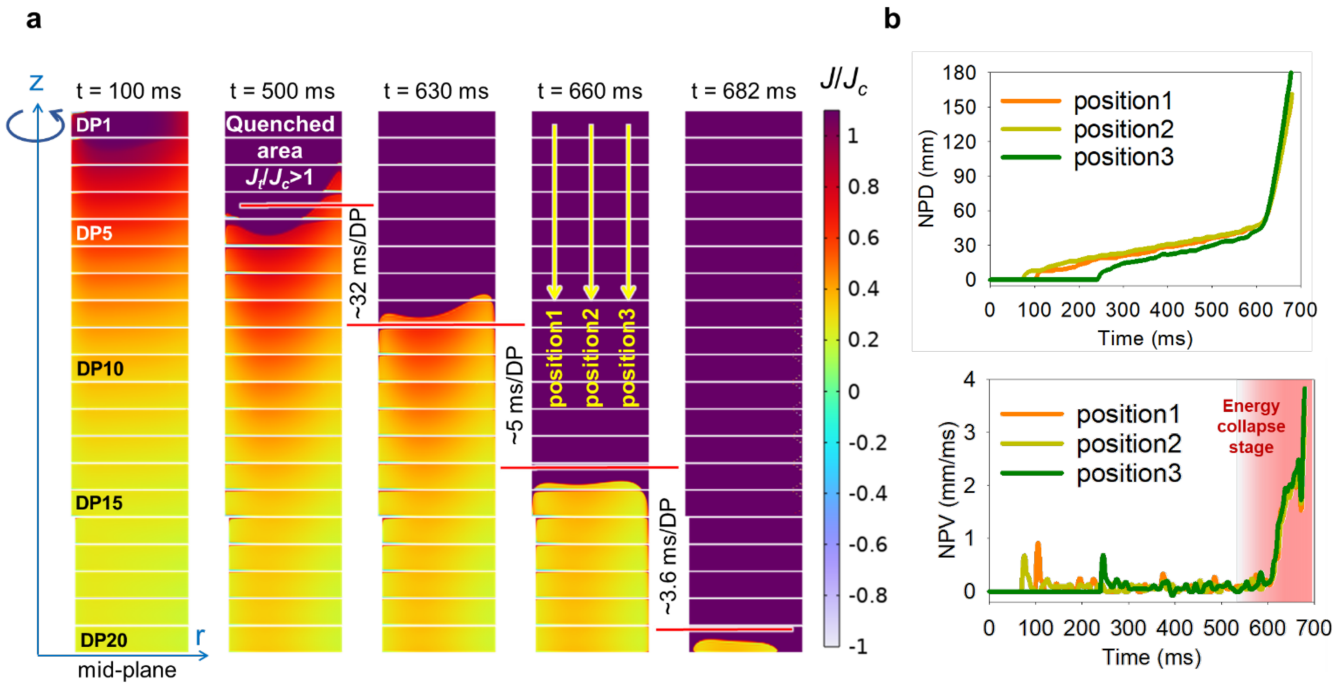

Fig.7 The simulated (a) *J*/*Jc* distribution during the unshunted H835 fault-mode quench propagation and (b) its corresponding normal-zone propagation distance (NPD) and normal-zone propagation velocity (NPV).

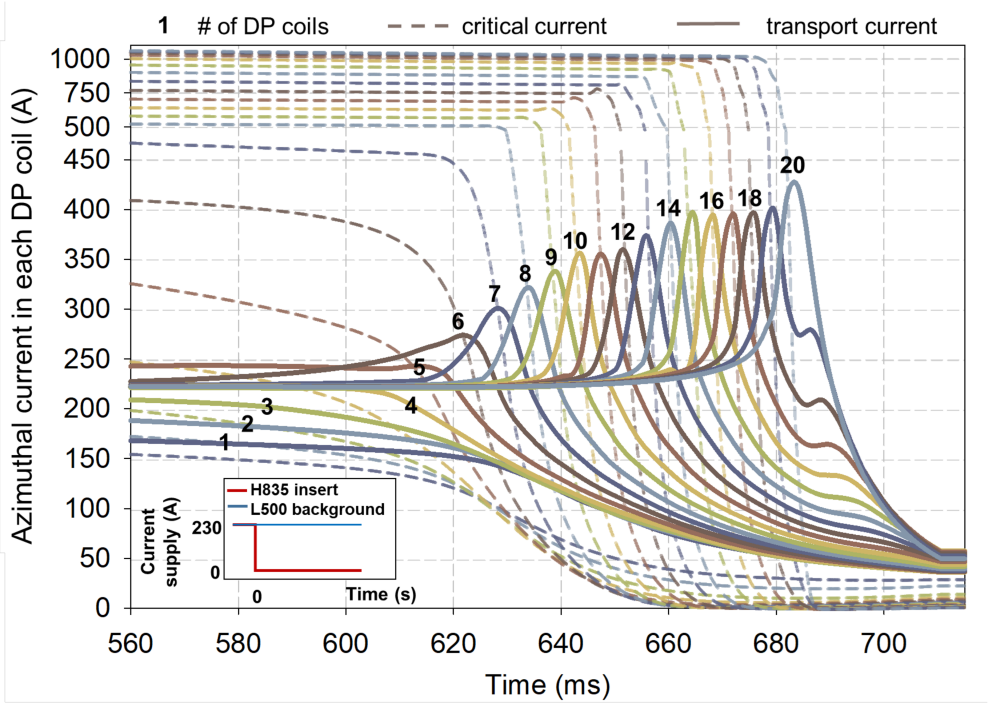

Fig.8 The simulated azimuthal current induction during the unshunted H835 fault-mode quench.

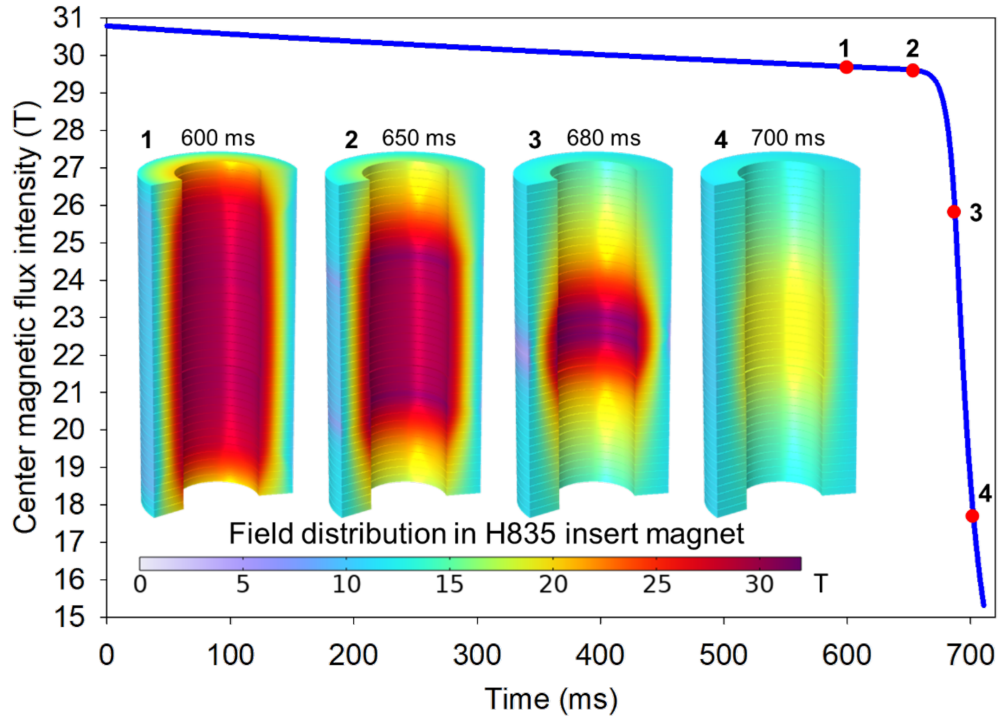

Fig.9 The simulated center magnetic field changes during the unshunted H835 fault-mode quench.

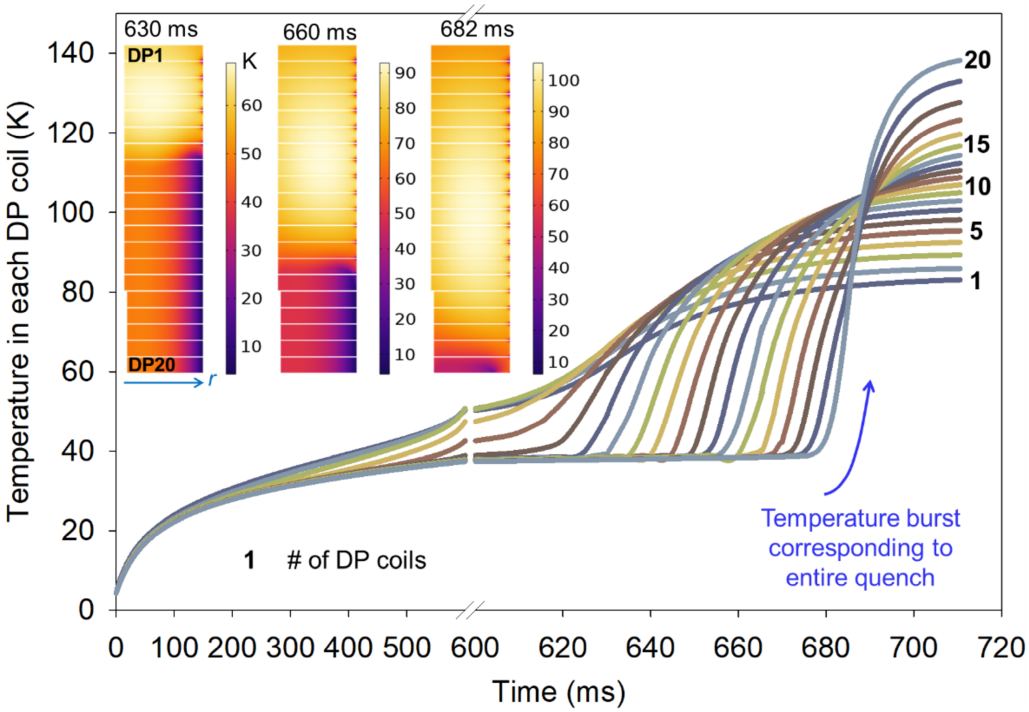

Fig.10 The simulated temperature changes during the unshunted H835 fault-mode quench.

Based on the above analysis of the unshunted case, we understand that to prevent the fault-mode quench, it is

crucial to suppress the thermal runaway in quench initiation and interrupt the induced current in quench propagation. To prove the effectiveness of the surface shunt in the fault-mode quench prevention, we assume in the simulation that the background magnet L500 also decays its field simultaneously when the fault mode occurs on the H835 insert magnet, which is the most severe operation condition because the decay of the background field will induce an extra current in addition to the existing overcurrent in the H835 quench. Fig.11a shows the distribution of the normalized current density (J/Jc) after H835 is shunted. Compared to the original unshunted one shown in Fig. 7a, the fault-mode quench is not only significantly delayed in initiation from millisecond level to second level (i.e., 100 ms vs. 10 s), but also interrupted in propagation up to ~DP12, starting to recover after t = 36 s. We further observe the changes of J/Jc in space and time, as Fig.11b shows, finding that J/Jc stays below 1 during the entire fault-mode event. This is a significant difference from the original unshunted H835 in which $J/Jc>1$. We also simulate the azimuthal current changes in each DP coil, as shown in Fig.12. The currents are induced from an initial 230 A to a maximum of 320 A at ~35 s, but after that, the current is successfully suppressed and smoothly decays to 0 A within ~1000 s, while the current induction in the unshunted case is much more drastic (Fig. 8). Fig. 13 is the simulated temperature changes. The maximum temperature is limited to ~17 K. However, the cause of the few peaks in the temperature curves is still unclear. The explanation may relate to the temperature-dependent characteristics of the turn-to-turn resistance[29, 49, 55, 56] and the shunt resistance: when temperatures fluctuate, the two in-parallel resistances undergo an electrical re-balance in sharing the overcurrent. Fig.14 shows the center field decays with a time constant fitted to be 228 s, which further proves that the magnet stably remains superconducting during the fault mode. Compared to the quenched field distribution in Fig.9, the non-quenched field decays much more uniformly throughout the entire magnet. The H835 with the surface shunt can be safely discharged in the fault mode.

Comparing the electromagnetic and thermal behaviors between the two cases, we find that the surface shunt effectively shares not only the turn-to-turn bypass current but also the induced current, thereby reducing the heat that triggers partial quench and the excessive overcurrent that propagates the quench. The turn-to-turn coupling is adjusted making the magnet more robust against the fault-mode quench.

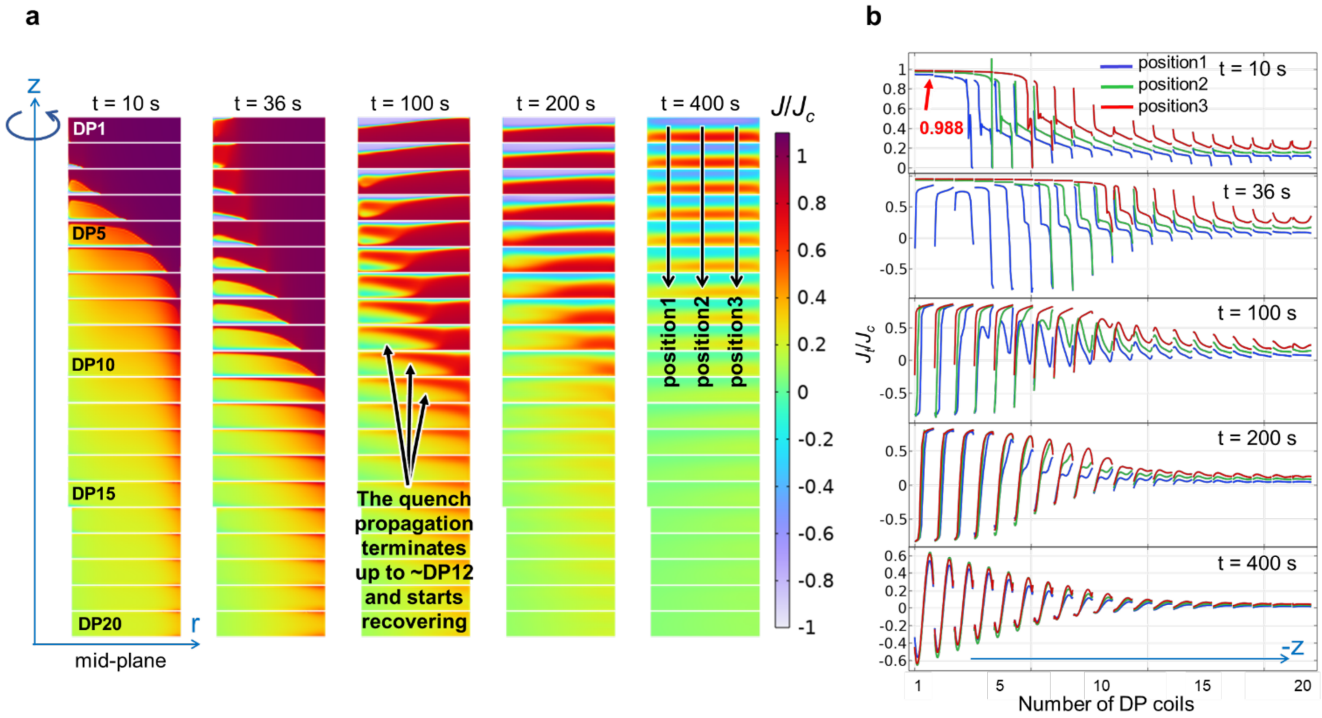

Fig.11 The simulated (a) *J*/*Jc* distribution during the shunted H835 in fault mode and (b) the detailed *J*/*Jc* with space and time.

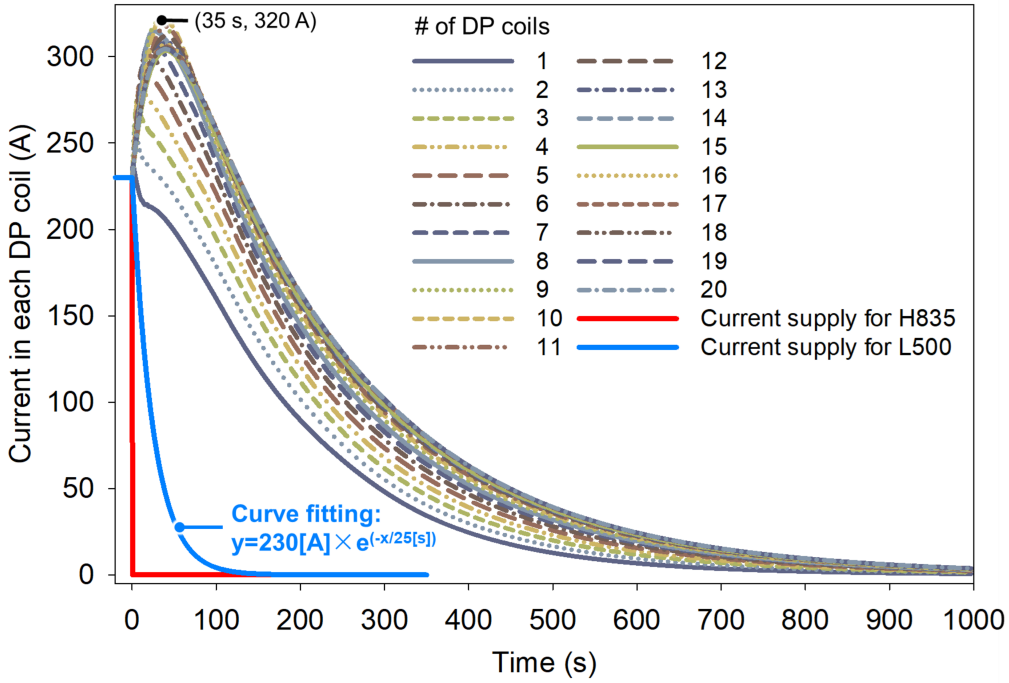

Fig.12 The simulated azimuthal current induction and decay in the shunted H835 in fault mode.

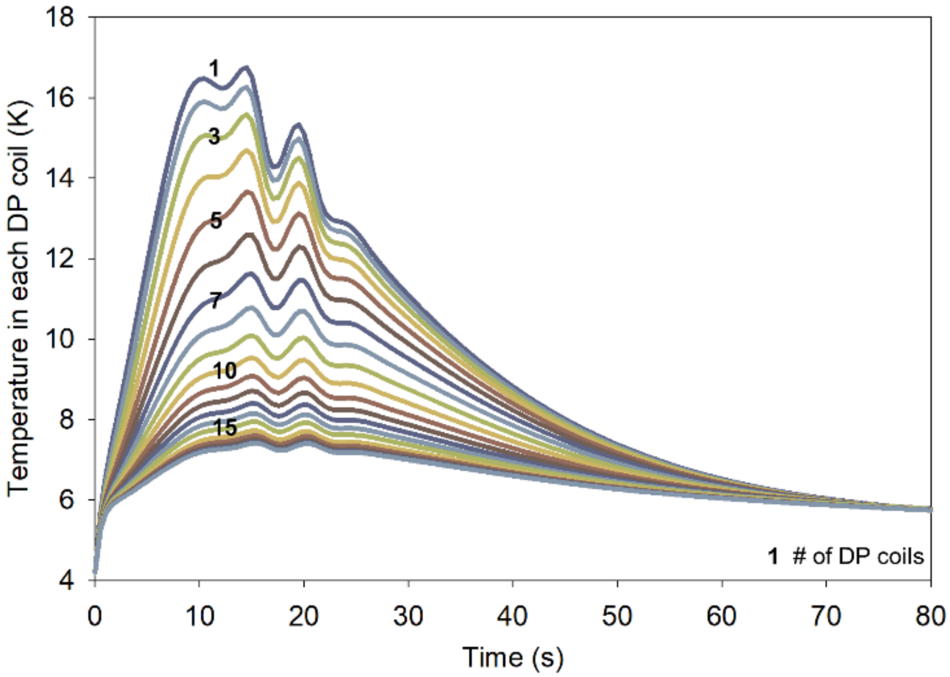

Fig.13 The simulated temperature changes in the shunted H835 in fault mode.

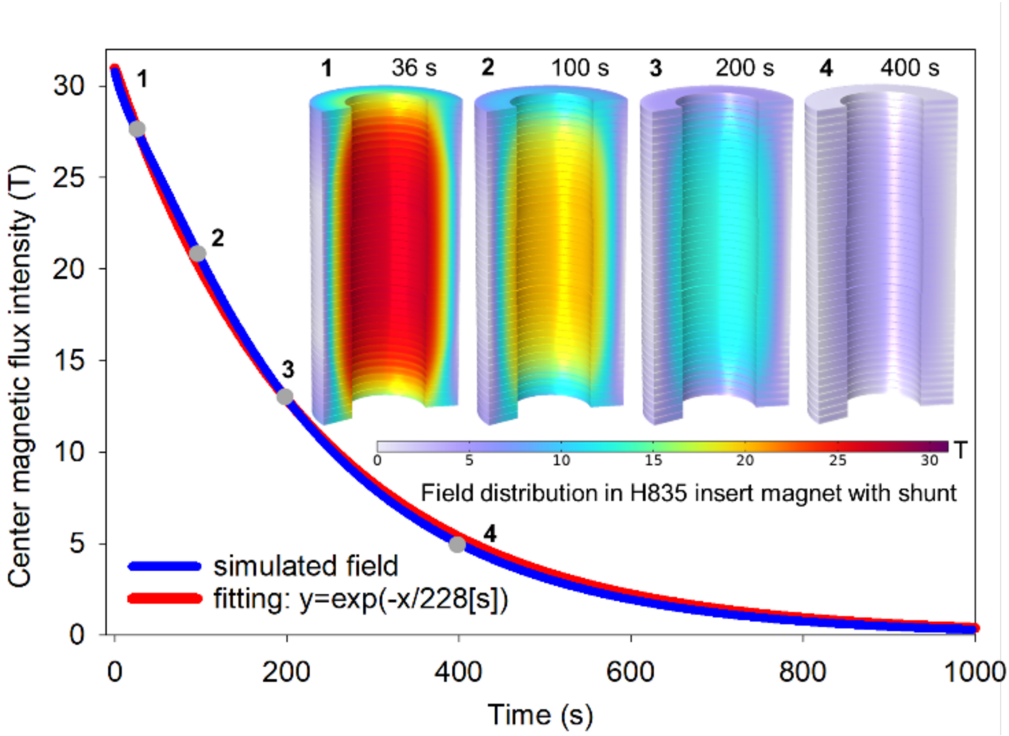

Fig.14 The simulated center magnetic field changes in the shunted H835 in fault mode.

5. Simulation on mechanical behaviors with and without the shunt

Besides the electromagnetic and thermal behaviors, we also performed a simulation to compare the mechanical

response in the fault-mode quench in both unshunted and shunted cases. The mechanical model is based on 2D axial symmetric static structure analyses, with the coils modeled turn-by-turn of HTS tape and co-wound stainless-steel tape. The bobbin of the coil is fixed, and the bottom boundary of the winding is set only axially fixed because of the support from the adjacent coils stack in *Z*-axis, and the whole winding volume is free to move radially and axially as the coil is 'dry-wound', that is, the coils are free of epoxy or any other encapsulant and therefore the individual coil turns within the winding are essentially 'self-supporting'. Then we applied to each turn with the current and magnetic field calculated from the above electromagnetic and thermal analyses, of which the current, including the screening current and overcurrent component, was acquired under local temperature- and field-dependent critical current *Ic*, and the field was acquired under this distribution of current.

Fig.15a shows the simulation results of stress/strain in the unshunted case, we selected DP1 as an example of end coil and DP17-20 as examples of middle coils in the magnet for the following reason: in the end coil, the screening current stress is usually the largest, while during fault-mode quench propagation to the middle coils, the induced overcurrent, as well as the unbalanced electromagnetic force, keep growing higher. Therefore, we mainly focus on the mechanical behaviors in these end and middle coils. In the fault mode, the quench initiation starts from end coils, firstly running out the *Ic* margin which is used for screening current. Consequently, the screening-current-induced stress (SCS) decreases. But in the middle coils, the overcurrent level keeps increasing, which induces a much higher stress than the SCS. The REBCO conductor tapes of the inner coil turns of these middle coils yield (the black area in the figure) during the fault-mode quench as the stress and strain levels have exceeded the allowable limits of 800 MPa and 0.55%, respectively, tested by our manufacturer[57-59]. In practical operation, stresses beyond the allowable level, typically 600–800 MPa, cannot be used in any case because the REBCO begins to degrade its critical current. The results indicate that the magnet could be damaged in the fault-mode quench. This destructive stress level is because the very high and uneven currents transiently induced in NI turns during the fault mode generate destructive-level stresses in the NI coil and huge unbalanced forces between coils. Considering that the H835 is 'dry-wound' without any support from epoxy or any other encapsulant, the effect just described is likely to induce relatively high in-winding stress, especially in the high field[60, 61].

Results of the shunted case (Fig. 15b) show that the electromagnetic force drops by almost 2/3 because the quench is suppressed and eliminated during the fault mode. The simulation results also show that the stress is <600 MPa and the strain is <0.5%, which will not cause any tape damage nor *Ic* degradation based on testing results by the REBCO manufacturer[57-59]. The delamination due to surface shunting is unlikely because the shunt material we use ($Bi_{49}Pb_{18}In_{21}Sn_{12}$) has very low bonding strength and did not cause any issues in our previous 25-T magnet[42].

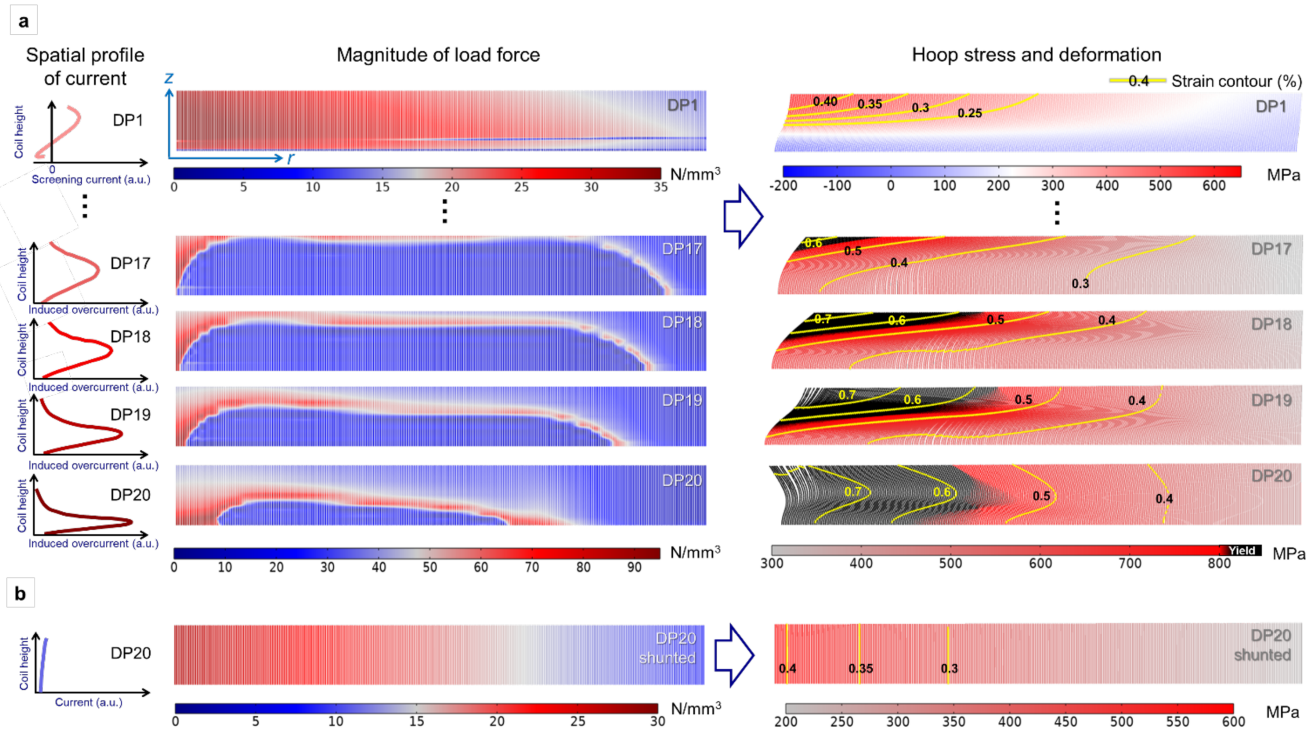

Fig.15 The simulated mechanical responses in the fault mode of the (a) unshunted and (b) shunted cases.

6. Discussions

The key feature of the surface shunt is to provide an additional current-releasing bypass located out of the NI winding pack to redirect the turn-to-turn bypass current, reducing the turn-to-turn resistance and thus joule heating during the fault mode, mitigating the consequent temperature increases and overstresses. Therefore, the magnet can be self-protective during the fault mode.

The proposed surface shunt is different from the conventional dump resistor. The role of a dump resistor is to dissipate the quench energy as fast as possible to avoid burnout in an insulated magnet, and it is designed mainly based on magnet stored energy and current decay rate (or, the bearable voltage for insulations)[62]. The surface shunt requires additional considerations on turn-to-turn heating, ambient cooling conditions, and magnetic coupling in NI winding. The circuit diagram (Fig. 16) shows the surface shunt does not intend to fast dump the magnet energy, but instead, shares overcurrent and diverts some portion of energy, to slow down the energy-releasing speed for an adequate time of ambient cooling during the fault mode.

The stored energy of DP0 is ~300 J. In the fault mode (a supplying current cut-off) test, the unshunted DP0 releases its energy in ~200 ms, thus the average releasing power $P_{release}$ is calculated to reach 1.5 kW. Considering the circumambient cryogen (solid nitrogen SN_2) has thermal diffusivity of 3-5 orders of magnitude less than that of copper and aluminum[62], the ambient cooling fails to take the heat away in time, leading to DP0 almost adiabatically heat up and consequently quench. Further thermal estimation indicates the ambient cooling capacity has a dozen

watts, and this requires that $P_{release}$ must be at a similar level for thermal equilibrium. Thus, the total energy-releasing time must be in a dozen seconds rather than milliseconds level. According to $R = L/\tau$, the equivalent turn-to-turn resistance R_{tt} must be less than a few milliohms. Practically, the R_{tt} of the shunted DP0 is tested to be 1.38 mΩ. The full-size H835 magnet containing 40 DPs has the same cooling structure as that of DP0. Therefore, the ambient cooling capacity is ~40 times larger (~500-700 W). We calculate that $P_{release}$ = 0.5×(230 A)²×(20.3 H [inductance])÷(900 s [energy-releasing time]) = ~600 W falls into this range when the shunt is applied, whereas for the unshunted H835, $P_{release}$ reaches to astounding 700 kW. We consider that practical R_{tt} equal to a few mΩ should be fine for this shunt as long as $P_{release}$ is not exaggerative, i.e., >10 times larger than the ambient cooling.

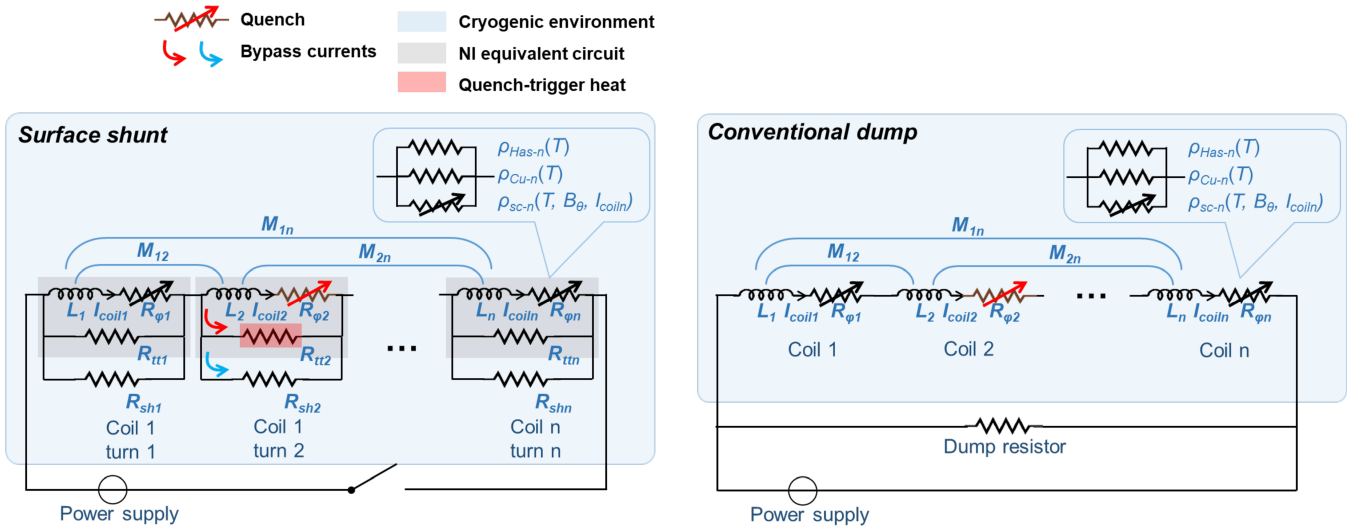

Fig.16 The circuit diagrams of the surface shunt and the conventional dump resistor. M: mutual inductance; L: self-inductance; I_{coil}: current in coil turns; R_{φ}: resistance from quench REBCO; R_{tt}: turn-to-turn resistance; R_{sh}: shunt resistance; ρ_{Has}, ρ_{Cu}, and ρ_{sc}: resistivity of Hastelloy substrate, copper, and REBCO layers in the HTS conductor, respectively.

Here, we also discuss the discrepancy between the experimental test and the simulation results at the end of the quench. In Fig.6a, the simulated magnetic field gradually saturates at 0.1 (normalized), while in the experiment, it can discharge completely to zero. This discrepancy was also observed in [29]. This discrepancy can be explained as: in practical tests, the quench does not always occur perfectly evenly along a coil turn as compared to that in the 2D axial symmetric simulation, this leads to some local quench happening dominantly within its small volume rather than the whole turn been warmed up by the azimuthal and radial currents, resulting in a higher current-sharing temperature *Tcs* of the small volume than that of the whole turn. The remained current (or residual magnetic field) in the test is thus less than that in the simulation. However, once a quench happens to a coil turn, either locally or not, the whole turn of azimuthal current fast reduces and the quench propagates out mainly relying on the electromagnetic coupling between turns. Therefore, this discrepancy due temperature factor only exists at the end of the quench, and

has very limited influence on the main quench process because electromagnetic coupling is the factor that dominates during the quench. It can be seen the simulation has a good match to the experiment in the main quench period that we are interested in.

7. Conclusions

In this work, we use a surface-shunting method for the prevention of quench in high-field no-insulation (NI) magnets composed of a stack of REBCO double pancakes, quench that is triggered by external failures of magnet current leads or power suppliers (i.e., the fault-mode). We report this quench and study its mechanism, finding that it initiates by turn-to-turn bypass current heat and spreads due to overcurrent induced by magnetic coupling in adjacent coils. Our surface shunting approach provides a current sharing bypass in addition to the existing NI turn-to-turn bypass, adjusting the turn-to-turn coupling by redirecting the current out of the winding pack. This effectively slows down the energy release and maintains the in-winding temperatures, currents, and stresses within safe ranges during fault mode, making the coils robust against this type of quench.

In practice, this surface shunt is flexible to apply even after completing and pre-testing the coils. It protects the magnet by simply attaching proper low-temperature solder or any very-thin shunting materials, such as indium or indium-tin ribbon, to the double pancake top/bottom surfaces. This method offers the following highly compatible merits of protection in both fault mode and internal defects: controllable parameter values and compact spatial volumes in applications of high-field HTS magnet systems. We believe the surface shunt method will offer a key solution to the critical issues in the safe operation of high-field large-scale HTS NI magnet systems.

Acknowledgments

This work was supported by the National Institute of General Medical Sciences of the National Institutes of Health under Award R01GM137138. This material is based upon work supported by the U.S. Department of Energy, Office of Science, Office of High Energy Physics under Award Number DE-SC0024025.

References

[1] Z. S. Hartwig, R. F. Vieira, D. Dunn, T. Golfinopoulos, B. LaBombard, C. J. Lammi, P. C. Michael, S. Agabian, D. Arsenault, R. Barnett, M. Barry, L. Bartoszek, W. K. Beck, D. Bellofatto, D. Brunner, W. Burke, J. Burrows, W. Byford, C. Cauley, S. Chamberlain, D. Chavarria, J. L. Cheng, J. Chicarello, V. Diep, E. Dombrowski, J. Doody, R. Doos, B. Eberlin, J. Estrada, V. Fry, M. Fulton, S. Garberg, R. Granetz, A. Greenberg, M. Greenwald, S. Heller, A. E. Hubbard, E. Ihloff, J. H. Irby, M. Iverson, P. Jardin, D. Korsun, S. Kuznetsov, S. Lane-Walsh, R. Landry, R. Lations, R. Leccacorvi, M. Levine, G. Mackay, K. Metcalfe, K. Moazeni, J. Mota, T. Mouratidis, R. Mumgaard, J. P. Muncks, R. A. Murray, D. Nash, B. Nottingham, C. O'Shea, A. T. Pfeiffer, S. Z. Pierson, C. Purdy, A. Radovinsky, D. K. Ravikumar, V. Reyes, N. Riva, R. Rosati, M. Rowell, E. E. Salazar, F. Santoro, A. Sattarov, W. Saunders, P. Schweiger, S. Schweiger, M. Shepard, S. Shiraiwa, M. Silveira, F. T. Snowman, B. N. Sorbom, P. Stahle, K. Stevens, J. Stillerman, D. Tammana, T. L. Toland, D. Tracey, R. Turcotte, K. Uppalapati, M. Vernacchia, C. Vidal, E. Voirin, A. Warner, A. Watterson, D. G. Whyte, S. Wilcox, M. Wolf, B. Wood, L. H.

Zhou, and A. Zhukovsky, “The SPARC Toroidal Field Model Coil Program,” *IEEE Transactions on Applied Superconductivity,* vol. 34, no. 2, Mar, 2024.

[2] F. L. Dong, L. N. Hao, D. Park, Y. Iwasa, and Z. Huang, “On the future sustainable ultra-high-speed maglev: An energy-economical superconducting linear thrusting system,” *Energy Conversion and Management,* vol. 291, Sep 1, 2023.

[3] D. Park, F. Dong, W. Lee, J. Bascuñán, and Y. Iwasa, “First-Cut Design of a Benchtop Cryogen-Free 23.5-T/25-mm Magnet for 1-GHz Microcoil NMR,” *IEEE Transactions on Applied Superconductivity,* vol. 33, no. 5, Aug, 2023.

[4] Y. Yanagisawa, M. Hamada, K. Hashi, and H. Maeda, “Review of recent developments in ultra-high field (UHF) NMR magnets in the Asia region,” *Superconductor Science & Technology,* vol. 35, no. 4, Apr 1, 2022.

[5] Q. L. Wang, J. H. Liu, J. X. Zheng, J. G. Qin, Y. W. Ma, Q. J. Xu, D. L. Wang, W. E. Chen, T. M. Qu, X. Y. Zhang, D. H. Jiang, Y. H. Wang, B. Z. Zhou, L. Qin, H. Jin, H. J. Liu, Y. J. Zhai, and F. Liu, “Progress of ultra-high-field superconducting magnets in China,” *Superconductor Science & Technology,* vol. 35, no. 2, Feb, 2022.

[6] L. Rossi, and C. Senatore, “HTS Accelerator Magnet and Conductor Development in Europe,” *Instruments,* vol. 5, no. 1, Feb, 2021.

[7] F. L. Dong, Z. Huang, L. N. Hao, X. Y. Xu, Z. J. Jin, and N. Shao, “An on-board 2G HTS magnets system with cooling-power-free and persistent-current operation for ultrahigh speed superconducting maglevs,” *Scientific Reports,* vol. 9, Aug 14, 2019.

[8] D. W. Hazelton, V. Selvamanickam, J. M. Duval, D. C. Larbalestier, W. D. Markiewicz, H. W. Weijers, and R. L. Holtz, “Recent Developments in 2G HTS Coil Technology,” *IEEE Transactions on Applied Superconductivity,* vol. 19, no. 3, pp. 2218-2222, Jun, 2009.

[9] S. Hahn, K. Kim, K. Kim, X. B. Hu, T. Painter, I. Dixon, S. Kim, K. R. Bhattarai, S. Noguchi, J. Jaroszynski, and D. C. Larbalestier, “45.5-tesla direct-current magnetic field generated with a high-temperature superconducting magnet,” *Nature,* vol. 570, no. 7762, pp. 496-499, Jun 27, 2019.

[10] J. H. Liu, Q. L. Wang, L. Qin, B. Z. Zhou, K. S. Wang, Y. H. Wang, L. Wang, Z. L. Zhang, Y. M. Dai, H. Liu, X. N. Hu, H. Wang, C. Y. Cui, D. G. Wang, H. Wang, J. S. Sun, W. S. Sun, and L. Xiong, “World record 32.35tesla direct-current magnetic field generated with an all-superconducting magnet,” *Superconductor Science & Technology,* vol. 33, no. 3, Mar, 2020.

[11] M. Breschi, L. Cavallucci, P. L. Ribani, A. V. Gavrilin, and H. W. Weijers, “Analysis of quench in the NHMFL REBCO prototype coils for the 32T Magnet Project,” *Superconductor Science & Technology,* vol. 29, no. 5, May, 2016.

[12] Z. Huang, F. L. Dong, X. Y. Xu, X. Y. Teng, W. Ren, J. J. Zhang, W. Li, G. T. Ma, and Z. J. Jin, “Evaluation of the Structural Dynamics of a 2G HTS Magnet System Considering Electromagnetic and Thermal Stress,” *IEEE Transactions on Applied Superconductivity,* vol. 31, no. 5, Aug, 2021.

[13] L. Ren, G. L. Chen, Y. Xu, D. S. Pu, J. Xu, S. N. A. Yan, J. Shi, and L. Chen, “Experimental Analysis of Quench Characteristic in HTS Tapes and Coils,” *IEEE Transactions on Applied Superconductivity,* vol. 29, no. 5, Aug, 2019.

[14] L. Y. Liu, Y. Chen, H. Y. Zhang, W. Chen, J. T. Shi, X. S. Yang, Y. Zhang, and Y. Zhao, “Quench Characteristics Comparison Between Solid Nitrogen and Conduction Cooled REBCO Coil Under Thermal Disturbance and Over Current Pulse,” *IEEE Transactions on Applied Superconductivity,* vol. 28, no. 4, Jun, 2018.

[15] D. H. Liu, D. K. Li, W. W. Zhang, H. D. Yong, and Y. H. Zhou, “Electromagnetic-thermal-mechanical behaviors of a no-insulation double-pancake coil induced by a quench in the self field and the high field,” *Superconductor Science & Technology,* vol. 34, no. 2, Feb, 2021.

[16] Y. Suetomi, T. Yoshida, S. Takahashi, T. Takao, G. Nishijima, H. Kitaguchi, Y. Miyoshi, M. Hamada, K. Saito, R. Piao, Y. Takeda, H. Maeda, and Y. Yanagisawa, “Quench and self-protecting behaviour of an intra-layer no-insulation (LNI) REBCO coil at 31.4 T,” *Superconductor Science & Technology,* vol. 34, no. 6, Jun, 2021.

[17] F. L. Dong, Z. Huang, X. F. Li, L. N. Hao, L. P. Yao, W. Wu, and Z. J. Jin, “R&D of No-Insulation HTS Magnets Using 2G Wires in a Prototype for Maglev Applications,” *IEEE Transactions on Applied Superconductivity,* vol. 29, no. 5, Aug, 2019.

[18] S. Hahn, Y. Kim, D. K. Park, K. Kim, J. P. Voccio, J. Bascunan, and Y. Iwasa, “No-insulation multi-width winding technique for high temperature superconducting magnet,” *Applied Physics Letters,* vol. 103, no. 17, Oct 21, 2013.

[19] W. K. Chan, and J. Schwartz, “Improved stability, magnetic field preservation and recovery speed in (RE)Ba2Cu3Ox-based no-insulation magnets via a graded-resistance approach,” *Superconductor Science & Technology,* vol. 30, no. 7, Jul, 2017.

[20] Y. Wang, W. K. Chan, and J. Schwartz, “Self-protection mechanisms in no-insulation (RE) Ba2Cu3Ox high temperature superconductor pancake coils,” *Superconductor Science & Technology,* vol. 29, no. 4, Apr, 2016.

[21] D. Qiu, Z. Y. Li, F. Gu, Z. Huang, A. Zhao, D. Hu, B. G. Wei, H. Huang, Z. Hong, K. Ryu, and Z. Jin, “Experiment study on an inductive superconducting fault current limiter using no-insulation coils,” *Physica C-Superconductivity and Its Applications,* vol. 546, pp. 1-5, Mar 15, 2018.

[22] D. Y. Hu, Y. Zhang, and K. Mao, “Design, Fabrication and Test of a High- Temperature Superconducting Linear Synchronous Motor Mover Magnet Prototype for High-Speed Maglev,” *IEEE Access,* vol. 10, pp. 111087-111104, 2022.

[23] F. L. Dong, Z. Huang, X. Y. Xu, L. N. Hao, N. Shao, and Z. J. Jin, “Improvement of magnetic and cryogenic energy preservation performances in a feeding-power-free superconducting magnet system for maglevs,” *Energy,* vol. 190, Jan 1, 2020.

[24] F. L. Dong, Z. Huang, X. Y. Xu, M. Y. Wang, X. Y. Teng, L. N. Hao, and Z. J. Jin, “Method and Process of Mechanical Evaluation of a 2G HTS Magnet System for Maglev Applications,” *IEEE Transactions on Applied Superconductivity,* vol. 30, no. 4, Jun, 2020.

[25] Y. H. Zhai, B. Berlinger, C. Barth, and C. Senatore, “Design, construction, and testing of no-insulation small subscale solenoids for compact tokamaks,” *Superconductor Science & Technology,* vol. 34, no. 10, Oct, 2021.

[26] N. Mitchell, J. X. Zheng, C. Vorpahl, V. Corato, C. Sanabria, M. Segal, B. Sorbom, R. Slade, G. Brittles, R. Bateman, Y. Miyoshi, N. Banno, K. Saito, A. Kario, H. Ten Kate, P. Bruzzone, R. Wesche, T. Schild, N. Bykovskiy, A. Dudarev, M. Mentink, F. J. Mangiarotti, K. Sedlak, D. Evans, D. C. Van Der Laan, J. D. Weiss, M. Liao, and G. Liu, “Superconductors for fusion: a roadmap,” *Superconductor Science & Technology,* vol. 34, no. 10, Oct, 2021.

[27] D. Park, J. Bascunan, Y. Li, W. Lee, Y. Choi, and Y. Iwasa, “Design Overview of the MIT 1.3-GHz LTS/HTS NMR Magnet with a New REBCO Insert,” *IEEE Transactions on Applied Superconductivity,* vol. 31, no. 5, Aug, 2021.

[28] Y. Iwasa, J. Bascunan, S. Hahn, J. Voccio, Y. Kim, T. Lecrevisse, J. Song, and K. Kajikawa, “A High-Resolution 1.3-GHz/54-mm LTS/HTS NMR Magnet,” *IEEE Transactions on Applied Superconductivity,* vol. 25, no. 3, Jun, 2015.

[29] K. R. Bhattarai, K. Kim, K. Kim, K. Radcliff, X. B. Hu, C. Im, T. Painter, I. Dixon, D. Larbalestier, S. Lee, and S. Hahn, “Understanding quench in no-insulation (NI) REBCO magnets through experiments and simulations,” *Superconductor Science & Technology,* vol. 33, no. 3, Mar, 2020.

[30] P. C. Michael, D. Park, Y. H. Choi, J. Lee, Y. Li, J. Bascunan, S. Noguchi, S. Hahn, and Y. Iwasa, “Assembly and Test of a 3-Nested-Coil 800-MHz REBCO Insert (H800) for the MIT 1.3 GHz LTS/HTS NMR Magnet,” *IEEE Transactions on Applied Superconductivity,* vol. 29, no. 5, Aug, 2019.

[31] J. Bascunan, S. Hahn, T. Lecrevisse, J. B. Song, D. Miyagi, and Y. Iwasa, “An 800-MHz all-REBCO Insert for the 1.3-GHz LTS/HTS NMR Magnet Program-A Progress Report,” *IEEE Transactions on Applied Superconductivity,* vol. 26, no. 4, Jun, 2016.

[32] Y. Li, D. Park, Y. F. Yan, Y. Choi, J. Lee, P. C. Michael, S. W. Chen, T. M. Qu, J. Bascunan, and Y. Iwasa, “Magnetization and screening current in an 800 MHz (18.8 T) REBCO nuclear magnetic resonance insert magnet: experimental results and numerical analysis,” *Superconductor Science & Technology,* vol. 32, no. 10, Oct, 2019.

[33] D. Park, J. Bascunan, P. C. Michael, J. Lee, Y. H. Choi, Y. Li, S. Hahn, and Y. Iwasa, “MIT 1.3-GHz LTS/HTS NMR Magnet: Post Quench Analysis and New 800-MHz Insert Design,” *IEEE Transactions on Applied Superconductivity,* vol. 29, no. 5, Aug, 2019.

[34] G. T. Ma, T. Y. Gong, R. C. Wang, S. L. Li, X. C. Nie, P. B. Zhou, J. Li, C. Li, Z. F. Ge, and H. B. Cui, “Design, fabrication and testing of a coated conductor magnet for electrodynamic suspension,” *Superconductor Science & Technology,* vol. 35, no. 2, Feb, 2022.

[35] Z. Jiang, H. Song, W. Song, and R. A. Badcocka, “Optimizing coil configurations for AC loss reduction in REBCO HTS fast-ramping magnets at cryogenic temperatures,” *Superconductivity,* vol. 3, pp. 100024, 2022.

[36] Z. L. Zhang, B. Z. Zhou, J. H. Liu, L. Wang, and Q. L. Wang, “Engineering-based design and fabrication procedure for mid-temperature

REBCO magnets accommodating the strong Ic anisotropy," *Superconductivity,* vol. 1, pp. 100005, 2022.

[37] Y. H. Wang, Q. L. Wang, J. H. Liu, J. S. Cheng, and F. Liu, "Insert magnet and shim coils design for a 27 T nuclear magnetic resonance spectrometer with hybrid high and low temperature superconductors," *Superconductor Science & Technology,* vol. 33, no. 6, Jun, 2020.

[38] S. Noguchi, D. Park, Y. Choi, J. Lee, Y. Li, P. C. Michael, J. Bascunan, S. Hahn, and Y. Iwasa, "Quench Analyses of the MIT 1.3-GHz LTS/HTS NMR Magnet," *IEEE Transactions on Applied Superconductivity,* vol. 29, no. 5, Aug, 2019.

[39] D. G. Whyte, B. LaBombard, J. Doody, T. Golfinopolous, R. Granetz, C. Lammi, S. Lane-Walsh, P. Michael, T. Mouratidis, R. Mumgaard, J. P. Muncks, D. Nash, N. Riva, F. Santoro, A. Sattarov, J. Stillerman, K. Uppalapati, R. Vieira, A. Watterson, S. Wilcox, and Z. S. Hartwig, "Experimental Assessment and Model Validation of the SPARC Toroidal Field Model Coil," *IEEE Transactions on Applied Superconductivity,* vol. 34, no. 2, Mar, 2024.

[40] F. L. Dong, D. Park, J. Kim, J. Bascuñán, and Y. Iwasa, "Sudden-Discharging Quench Dynamics in a No-Insulation Superconducting Coil," *IEEE Transactions on Applied Superconductivity,* vol. 33, no. 5, Aug, 2023.

[41] F. L. Dong, D. K. Park, W. Lee, L. N. Hao, Z. Huang, J. Bascuñán, Z. J. Jin, and Y. Iwasa, "On fault-mode phenomenon in no-insulation superconducting magnets: A preventive approach," *Applied Physics Letters,* vol. 121, no. 19, Nov 7, 2022.

[42] W. Lee, D. Park, J. Bascuñán, and Y. Iwasa, "Construction and test result of an all-REBCO conduction-cooled 23.5 T magnet prototype towards a benchtop 1 GHz NMR spectroscopy," *Superconductor Science & Technology,* vol. 35, no. 10, Oct 1, 2022.

[43] Y. Tsui, R. Mahmoud, E. Surrey, and D. Hampshire, "Superconducting and Mechanical Properties of Low-Temperature Solders for Joints," *IEEE Transactions on Applied Superconductivity,* vol. 26, no. 3, Apr, 2016.

[44] P. Bruzzone, "Electrical-Properties of Low Melting-Point Alloys at 4.2-K," *Cryogenics,* vol. 27, no. 8, pp. 433-435, Aug, 1987.

[45] R. C. Mataira, M. D. Ainslie, R. A. Badcock, and C. W. Bumby, "Finite-element modelling of no-insulation HTS coils using rotated anisotropic resistivity," *Superconductor Science & Technology,* vol. 33, no. 8, Aug, 2020.

[46] S. Otten, J. ter Harmsel, M. Dhalle, and H. Ten Kate, "Calculation and measurement of coupling loss in a no-insulation ReBCO racetrack coil exposed to AC magnetic field," *Superconductor Science & Technology,* vol. 36, no. 4, Apr 1, 2023.

[47] J. R. Olatunji, H. W. Weijers, N. M. Strickland, and S. C. Wimbush, "Modelling the Quench Behavior of an NI HTS Applied-Field Module for a Magnetoplasmadynamic Thruster Undergoing a 1kW Discharge," *IEEE Transactions on Applied Superconductivity,* vol. 33, no. 5, Aug, 2023.

[48] P. Duan, Y. Xu, Z. X. Yang, L. Ren, J. D. Li, J. Shi, and Y. J. Tang, "A Numerical Method for Transient Thermal Analysis of No-Insulation REBCO Pancake Coils With Several Resistive Joints," *IEEE Transactions on Applied Superconductivity,* vol. 33, no. 7, Oct, 2023.

[49] J. Bang, A. Musso, N. Riva, J. T. Lee, G. Kim, W. Jang, and S. Hahn, "Experiment and Analysis on Temperature-Dependent Electric Contact Resistivity of an NI HTS Coil," *IEEE Transactions on Applied Superconductivity,* vol. 33, no. 5, Aug, 2023.

[50] J. Harmsel, S. Otten, M. Dhalle, and H. ten Kate, "Magnetization loss and transport current loss in REBCO racetrack coils carrying stationary current in time-varying magnetic field at 4.2 K," *Superconductor Science & Technology,* vol. 36, no. 1, Jan 1, 2023.

[51] P. Duan, Y. Xu, L. Ren, J. D. Li, S. Q. Guo, J. Shi, and Y. J. Tang, "Transient Electromagnetic and Mechanical Analysis of No-Insulation Insert Coil Based on 2-D Method," *IEEE Transactions on Applied Superconductivity,* vol. 32, no. 8, Nov, 2022.

[52] B. Y. Shen, F. Grilli, and T. Coombs, "Overview of H-Formulation: A Versatile Tool for Modeling Electromagnetics in High-Temperature Superconductor Applications," *IEEE Access,* vol. 8, pp. 100403-100414, 2020.

[53] F. L. Dong, Z. Huang, D. R. Qiu, M. Y. Wang, A. F. Zhao, B. B. Zhu, L. B. Wang, and Z. J. Jin, "Studies on the features of characteristic resistance of a no-insulation superconducting coil in energizing and de-energizing processes," *Physica C-Superconductivity and Its Applications,* vol. 551, pp. 33-40, Aug 15, 2018.

[54] X. D. Wang, S. Hahn, Y. Kim, J. Bascunan, J. Voccio, H. Lee, and Y. Iwasa, "Turn-to-turn contact characteristics for an equivalent circuit model of no-insulation ReBCO pancake coil," *Superconductor Science & Technology,* vol. 26, no. 3, Mar, 2013.

[55] J. Lu, J. Levitan, D. McRae, and R. Walsh, "Contact resistance between two REBCO tapes: the effects of cyclic loading and surface

coating," *Superconductor Science & Technology,* vol. 31, no. 8, Aug, 2018.

[56] J. Lu, R. Goddard, K. Han, and S. Hahn, "Contact resistance between two REBCO tapes under load and load cycles," *Superconductor Science & Technology,* vol. 30, no. 4, Apr, 2017.

[57] Y. F. Zhang, M. Kasahara, A. Sundaram, P. Brownsey, A. Knoll, H. Kuraseko, and D. W. Hazelton, "Detailed studies of tensile and delamination properties of REBCO coated conductors," *8th Workshop on Mechanical and Electromagnetic Properties of Composite Superconductors (MEM 2016), Tallahassee, FL, USA*, 2016.

[58] Y. Zhang, D. W. Hazelton, R. Kelley, M. Kasahara, R. Nakasaki, H. Sakamoto, and A. Polyanskii, "Stress-Strain Relationship, Critical Strain (Stress) and Irreversible Strain (Stress) of IBAD-MOCVD-Based 2G HTS Wires Under Uniaxial Tension," *IEEE Transactions on Applied Superconductivity,* vol. 26, no. 4, Jun, 2016.

[59] D. W. Hazelton, "2G HTS Properties Beyond Critical Current," *CHATS on Applied Superconductivity, Cambridge, MA, USA*, 2013.

[60] Y. F. Yan, D. H. Jiang, P. Song, J. Park, S. Hahn, Y. F. Tan, and T. M. Qu, "Screening-current-induced magnetic fields and strains in a compact REBCO coil in self field and background field," *Superconductivity,* vol. 9, Mar, 2024.

[61] P. F. Gao, M. Z. Guan, X. Z. Wang, and Y. H. Zhou, "Electromagnetic-thermal-structure multi-layer nonlinear elastoplastic modelling study on epoxy-impregnated REBCO pancake coils in high-field magnets," *Superconductivity,* vol. 1, Mar, 2022.

[62] Y. Iwasa, *Case Studies in Superconducting Magnets: Design and Operational Issues*, 2nd ed.: Springer, 2009.